ACS APPLIED MATERIALS & INTERFACES

Research Article

www.acsami.org

Improvements in the Electrochemical Kinetic Properties and Rate Capability of Anatase Titanium Dioxide Nanoparticles by Nitrogen Doping

Yongquan Zhang,[†] Fei Du,[†] Xiao Yan,[†] Yuming Jin,[†] Kai Zhu,[†] Xue Wang,[†] Haoming Li,[†] Gang Chen,[†,‡] Chunzhong Wang,[†,‡] and Yingjin Wei*[,†]

[†]Key Laboratory of Physics and Technology for Advanced Batteries (Ministry of Education), College of Physics, Jilin University, Changchun 130012, People's Republic of China

[‡]State Key Laboratory of Superhard Materials, Jilin University, Changchun 130012, People's Republic of China

ABSTRACT: Pure anatase TiO_2 and N-doped TiO_2 nanoparticles were prepared by a solvothermal method. X-ray photoelectron spectroscopy showed that the surface of the doped material was dominated by interstitial N, while interstitial and substitutional N coexisted in the material bulk. Both materials showed superior cycle stability. In addition, the N-doped material exhibited much better rate capability than pure TiO_2. A discharge capacity of 45 mAh g^{-1} was obtained at the 15 C rate, which was 80% higher than that of pure TiO_2. The electrochemical kinetic properties of the materials were studied by a galvanostatic intermittent titration technique and electrochemical impedance spectroscopy. The charge-transfer resistance of TiO_2 was decreased by N doping. Meanwhile, the minimum lithium diffusion coefficient was increased to 2.14×10^{-11} cm^2 s^{-1}, which is 13 times higher than that of pure TiO_2. This indicates that the electrochemical kinetic properties of TiO_2 were improved by N doping, which substantially improved the specific capacity and rate capability of TiO_2.

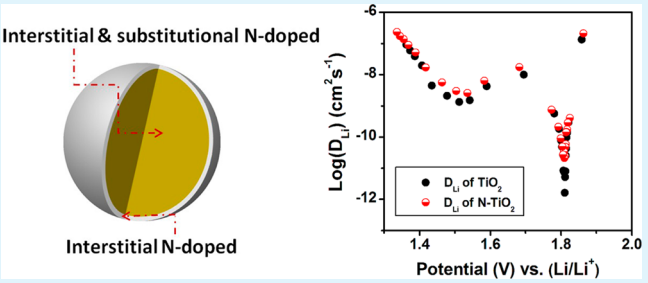

KEYWORDS: *lithium-ion battery, anatase titanium dioxide, N doping, rate capability, electrochemical kinetic properties*

1. INTRODUCTION

Lithium-ion batteries have been widely used in portable electronics. They are also considered to be one of the most promising power sources for electrical vehicles and stationary energy storage in the near future. For these new applications, a further decrease in cost and improvements in energy/power densities, safety, cycle life, and environmental impact are strongly required. Currently, graphite and other carbonaceous materials are the most commonly used anode materials in lithium-ion batteries. However, this kind of anode has severe safety issues because it operates close to the Li^+/Li redox couple with a risk of metallic lithium plating and dendrite formation at the overcharged state. In addition, it suffers from a high irreversible capacity loss during the initial cycles because of the formation of a solid electrolyte interphase film. Therefore, new anode materials with enhanced electrochemical performance are strongly required for lithium-ion batteries.

Recently, anatase titanium dioxide (TiO_2) has attracted great interest as the anode material for lithium-ion batteries because of its long cycle life, low cost, and minimum environmental impact.[1] Especially, the higher working voltage of TiO_2 (~1.6 V vs Li/Li^+) endows it with greater overcharge protection than the traditional graphite anode, which significantly improves the safety properties of the batteries. However, the poor rate capability of TiO_2 seriously hinders its practical applications in lithium-ion batteries. The rate capability of electrode materials mainly depends on their electrochemical kinetic properties at the electrode/electrolyte interface, as well as their bulk properties such as diffusion of Li^+ ions and electrical conductivity. In order to improve the electrochemical kinetic properties at the electrode/electrolyte interface, numerous works have been done to monitor the surface of TiO_2 by the preparation of mesoporous materials, or coating of the material with carbon, polypyrrole, RuO_2, etc.[2−9] In order to facilitate the diffusion of Li^+ ions, it is a common practice to prepare nanosized materials. Even though the intrinsic Li^+ ion diffusivity of TiO_2 is rather low, the nanosized material provides a short diffusion length, thus effectively shortening the diffusion time of Li^+ ions.[10] There are also different methods that can improve the electrical conductivity of TiO_2. For example, TiO_2 composites with electronic conductive additives such as carbon nanotubes, graphene, and RuO_2 have demonstrated an increased Li^+ ion capacity at high charge−discharge rates.[10−12] However, the conductive additives can only tailor electron transport on the particle surface and between adjacent particles; the intrinsic electrical conductivity inside the TiO_2

Received: January 11, 2014
Accepted: March 5, 2014
Published: March 5, 2014

   dx.doi.org/10.1021/am5002053 | *ACS Appl. Mater. Interfaces* 2014, 6, 4458−4465

bulk is still poor. Recently, it has been shown that the intrinsic electrical conductivity of TiO_2 can be improved by doping of some aliovalent ions such as Nb^{5+}, P^{5+}, Zn^{2+}, Fe^{3+}, N^{3-}, S^{2-}, and F^-.[13−21] In addition, slight modification of the TiO_2 lattice is achieved by doping of foreign atoms, which may improve the diffusion of Li^+ ions. For example, Kim et al. prepared N-doped TiO_2 nanofibers by the electrospining method. The N-doped nanofibers showed a discharge capacity of 185 mAh g^{-1} at the 0.1 C rate, which was much higher than that of the undoped counterpart.[17] Han et al. reported that the discharge capacity of their N-doped TiO_2 hollow nanofibers (85 mAh g^{-1}) was nearly 2 times higher than that of the ordinary TiO_2 nanoparticles at the 2C rate.[16] Liu et al. prepared N- and S-codoped TiO_2 nanocrystals. The material showed superior high rate performance because of increasing electrical conductivity.[20]

Because the diffusion of Li^+ ions in the electrode is a key step for energy storage and output, the chemical diffusion coefficient of Li^+ (D_{Li}) is one of the most important kinetic parameters for electrode materials. The galvanostatic intermittent titration technique (GITT), which is based on the chronopotentiometry at nearly thermodynamic equilibrium conditions, is a reliable technique to determine D_{Li} with highly resolved data. Electrochemical impedance spectroscopy (EIS) is also a powerful technique to determine D_{Li} because the low-frequency Warburg region is directly related to Li^+ diffusion in the electrode. Recently, the chemical diffusion coefficients of different electrode materials such as $Li[Li_{0.23}Co_{0.3}Mn_{0.47}]O_2$, $LiFeSO_4F$, $Li[Ni_{0.5}Mn_{0.3}Co_{0.2}]O_2$, and $LiCoO_2$ have been studied by several groups.[22−25] However, there is still a lack knowledge on the chemical diffusion coefficient of TiO_2 and its variation with the Li^+ content or working voltage. In this study, we prepared N-doped TiO_2 nanoparticles by a solvothermal method. The effects of N doping on the electrochemical properties of TiO_2, especially their electrochemical kinetic properties, were studied by GITT and EIS techniques.

2. EXPERIMENTAL SECTION

2.1. Synthesis and Characterization. Anatase TiO_2 nanoparticles were prepared by a solvothermal method. In brief, 12 mL of tetrabutyl titanate was dissolved in 48 mL of 2-butoxyethanol and 12 mL of acetic acid. After magnetic stirring for 1 h at room temperature, the resultant solution was placed in a 100 mL stainless steel autoclave and then heat-treated at 150 °C for 10 h. After solvothermal preparation, the autoclave was cooled naturally to room temperature, followed by washing several times with deionized water and acetone. The resultant powder was dispersed under ultrasonication in deionized water and then subjected to freeze-drying. Finally, the precursor powder was annealed at 550 °C for 5 h in air to obtain the pristine TiO_2 material. For the preparation of N-doped TiO_2, the TiO_2 precursor obtained from a solvothermal procedure was first annealed at 550 °C for 2 h in air, followed by another heat treatment at 550 °C under a NH_3 flow for 2 h. Finally, the N-doped TiO_2 was annealed at 550 °C for 1 h in air.

The crystal structures of the samples were studied by X-ray diffraction (XRD) on a Bruker AXS D8 X-ray diffractometer with Cu Kα radiation. The lattice parameters were calculated using the *Celref* 3 Program. The morphology of the materials was observed by scanning electron microscopy (SEM; Hitachi SU8020). X-ray photoelectron spectroscopy (XPS) was performed on a VG scientific ESCALAB 250 spectrometer. The binding energy was corrected using the C 1s peak at 284.6 eV.

2.2. Electrochemical Measurements. The electrochemical experiments were carried out using 2032-type coin cells. A metallic Li foil was used as the anode electrode. The cathode electrode was composed of 75 wt % active material, 15 wt % carbon black conductive additive, and 10 wt % poly(vinylidene fluoride) binder dissolved in *N*-methyl-2-pyrrolidone. The cathode slurry was coated on Al foil. Each electrode was 8 × 8 mm^2 in size with a TiO_2 mass loading of ~4 mg cm^{-2}. The cathode and anode electrodes were separated by the Celgard 2320 membrane. The electrolyte used was 1 mol L^{-1} lithium hexafluorophosphate dissolved in ethylene carbonate (EC), dimethyl carbonate (DMC), and ethyl methyl carbonate (EMC) [EC:DMC:EMC = 1:1:8 (w/w/w) ratio]. Galvonostatic charge−discharge cycling was performed on a Land-2100 battery tester. Cyclic voltammetry (CV), EIS, and GITT were performed on a Bio-Logic VSP multichannel potentiostatic−galvanostatic system. The impedance data were recorded by applying an alternating-current voltage of 5 mV in the frequency range from 1 MHz to 5 mHz. GITT measurement was performed throughout the discharge process. For each GITT step, the battery was discharged with a current flux of 16.8 mA g^{-1} for 0.5 h, followed by an open-circuit stand for 3 h to reach the quasi-equilibrium state.

3. RESULTS AND DISCUSSION

3.1. Structure and Morphology Properties. Figure 1 shows the XRD patterns of the TiO_2 and N-doped TiO_2 samples. Both materials can be indexed to anatase TiO_2 with the space group $I4_1/amd$ (JCPDS no. 21-1272). The lattice parameters of the materials are calculated as a = 3.7883 Å, b = 3.7883 Å, c = 9.5233 Å, and V = 136.67 $Å^3$ for pure TiO_2 and a = 3.7905 Å, b = 3.7905 Å, c = 9.5331 Å, and V = 136.97 $Å^3$ for N-doped TiO_2. The slight expansion of the crystal lattice may be due to the larger N^{3-} anion (r = 1.46 Å) than O^{2-} (r = 1.36 Å).[26] The narrow and sharp diffraction peaks indicate that the samples are well-crystallized. The average crystallite size (d) of the materials is calculated using Scherrer's formula,[27] $D = K\lambda/B\cos\theta$, where λ is the wavelength of the X-ray radiation, B is the angular width at half of the maximum intensity of the (101) peak, θ is the Bragg angle of the (101) peak, and K is a constant, which is 0.9. Calculation shows that the average crystallite size of pure TiO_2 (21.1 nm) is a little bit larger than that of N-doped TiO_2 (20.2 nm).

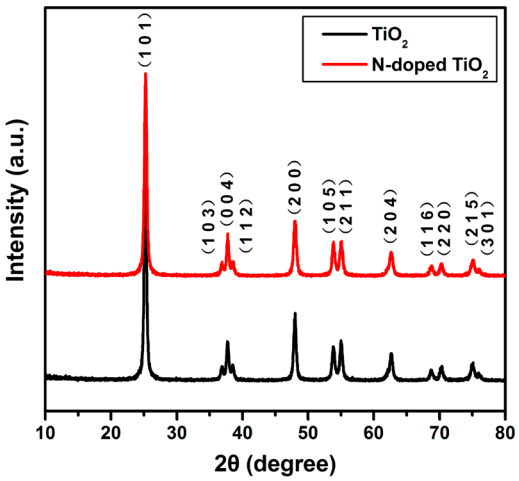

Figure 1. XRD patterns of the TiO_2 and N-doped TiO_2 samples.

The color of the TiO_2 powders changes from white to pale yellow after N doping. SEM shows that both samples have similar morphologies, as shown in Figure 2. The materials are composed of ordinary spherical-like particles with particle size of less than 50 nm. However, significant particle agglomeration is observed, which is difficult to resolve using the present synthetic route.

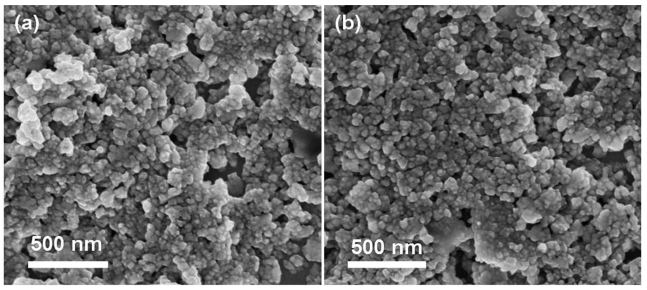

Figure 2. SEM images of the TiO_2 (a) and N-doped TiO_2 (b) samples.

3.2. XPS. XPS analysis was performed to investigate the chemical states of Ti, O, and N of the materials. As shown in Figure 3a,b, both the TiO_2 and N-doped TiO_2 samples exhibit very similar Ti 2p and O 1s XPS curves no matter the peak shape or the binding energies. The Ti 2p binding energy is observed at 458.4 eV, which is consistent with that of Ti^{4+}.[26] The O 1s binding energy at 529.6 eV confirms the O^{2-} state of the materials.[26] The existence of N 1s XPS confirms the successful doping of N in TiO_2. The amount of N dopant in the N-doped TiO_2 is measured as 1.17 atom %. In order to obtain detailed information on the chemical state of N in the material bulk, the N-doped TiO_2 sample was etched by Ar and then subjected to XPS analysis. Evolution of the N 1s XPS with Ar etching is displayed in Figure 3c. N 1s XPS at the sample surface is dominated by a single peak at 400.0 eV, which is attributed to the interstitial N anions in TiO_2 with an O−Ti−N linkage.[28] When the material is etched for 360 s, the O−Ti−N peak decreases while a new peak appears at 396.8 eV. This new peak is assigned to the Ti−N bond in TiN.[29,30] This indicates that some of the O atoms are substituted by N, which generates the direct linkage of the Ti and N atoms. The interstitial O−Ti−N bond shows a higher binding energy than that of the substituted Ti−N bond because the high electronegativity of O reduces the electron density on N. Both the O−Ti−N and Ti−N bonds can be observed with further etching, which confirms the coexistence of interstitial and substitutional N in the TiO_2 bulk. It has been reported that the site of N in the TiO_2 lattice depends on the synthetic history of the material.[28] Interstitial N is preferred under O-rich annealing conditions, whereas substitutional N is favored under O-depleted conditions. In this study, the N-doped TiO_2 is prepared by annealing the precursor in air. Therefore, the surface of the material is dominated by interstitial N atoms, while there are plenty of substitutional N atoms in the material bulk. The role of N on the electrical conductivity of TiO_2 is mainly related to the narrowing of the band gap. It has been reported that substitutional N plays a key role in narrowing the band gap by elevating the valence band maximum, while interstitial N can only introduce some localized N 2p states in the gap.[20]

3.3. Charge−Discharge Cycling. The electrochemical properties of the materials were studied in the voltage window of 1.3−3.0 V. The charge−discharge experiments were first performed at the 0.2 C rate (1C = 168 mA g^{-1}), and then the charge−discharge rate was gradually increased to 15 C. Figure 4 shows the voltage profiles of the materials at different charge−discharge rates. It has been well-accepted that Li^+ intercalation into TiO_2 undergoes a two-phase transition between the tetragonal TiO_2 and orthorhombic $Li_{0.5}TiO_2$ phases.[31] This means that the TiO_2 phase continuously decreases while the $Li_{0.5}TiO_2$ phase spontaneously increases with Li^+ intercalation. Normally, the charge−discharge profiles exhibit a voltage plateau under the two-phase mechanism, as observed in our undoped and N-doped TiO_2 samples. The theoretical capacity with 0.5 mol of Li^+ insertion into TiO_2 is 168 mAh g^{-1}. Recently, someone reported that the end phase of the two-phase transition is $Li_{0.55}TiO_2$.[32] There are no substantial differences between the two point of views, but the later one gives a slightly higher theoretical capacity of 185 mAh g^{-1}. In this study, the discharge capacities of the TiO_2 and N-doped TiO_2 samples at the 0.2 C rate are 170.6 and 181.7 mAh g^{-1}, respectively, which fit well with the above two-phase transition mechanisms. It has been reported that for nano- or mesoporous TiO_2 materials interfacial Li^+ ion storage is not negligible, which will give an extra discharge capacity.[33] However, this seems to not happen for our TiO_2 and N-doped TiO_2 samples because they have relatively large particle size and serious particle agglomeration, as observed from the SEM images.

The charge−discharge cycling performance of TiO_2 and N-doped TiO_2 at the 0.2 C rate is displayed in Figure 5. Both samples exhibit superior cycle stability in that only very small capacity fade is recorded after 100 cycles. The Columbic efficiency remains at nearly 100% after the initial cycles, which is an indication of excellent electrochemical reversibility. The rate-dependent cycling performance of the samples is displayed in Figure 6. It is clear that N-doped TiO_2 exhibits better rate capability than pure TiO_2, especially at higher charge−discharge

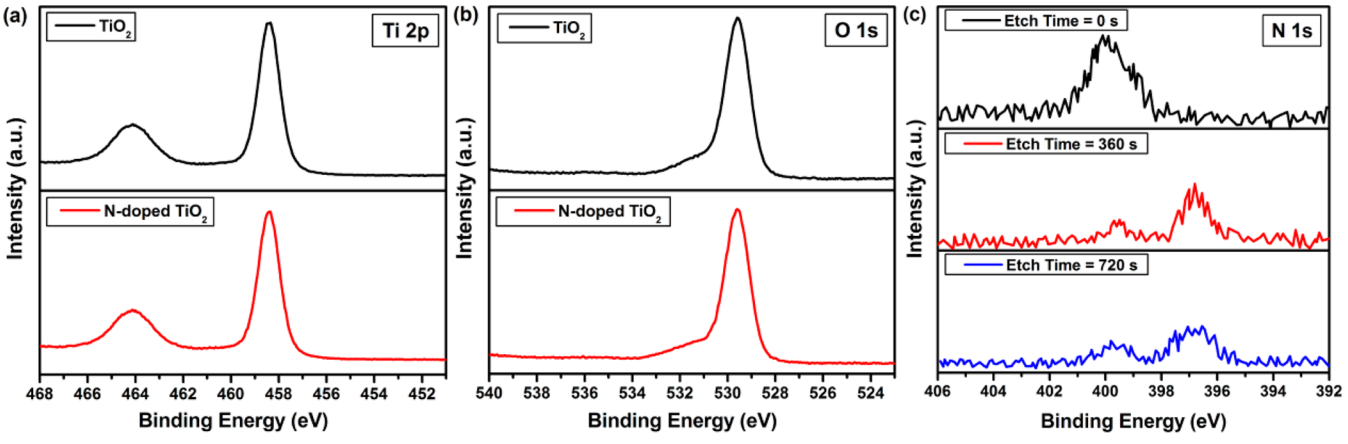

Figure 3. Ti 2p (a), O 1s (b), and N 1s (c) XPS of the TiO_2 and N-doped TiO_2 samples.

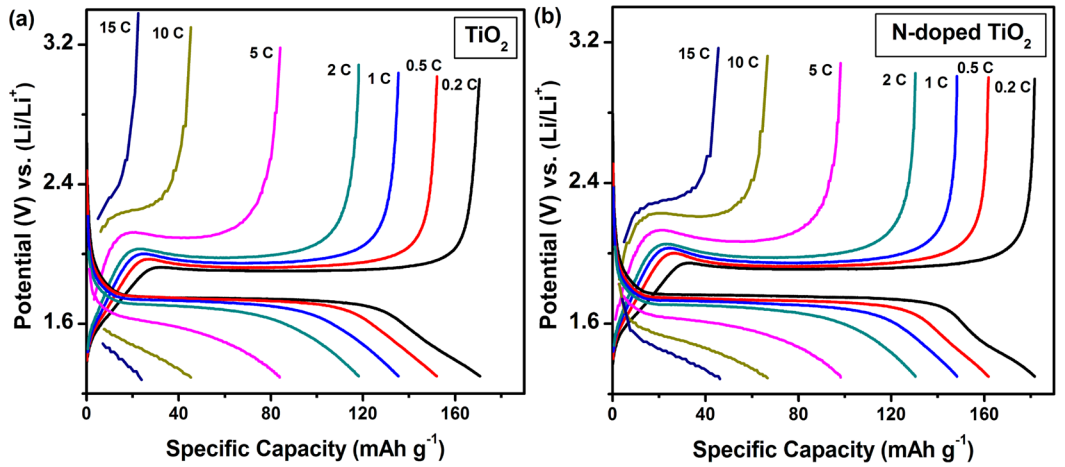

Figure 4. Voltage profiles of the TiO_2 (a) and N-doped TiO_2 (b) samples at different cycle rates.

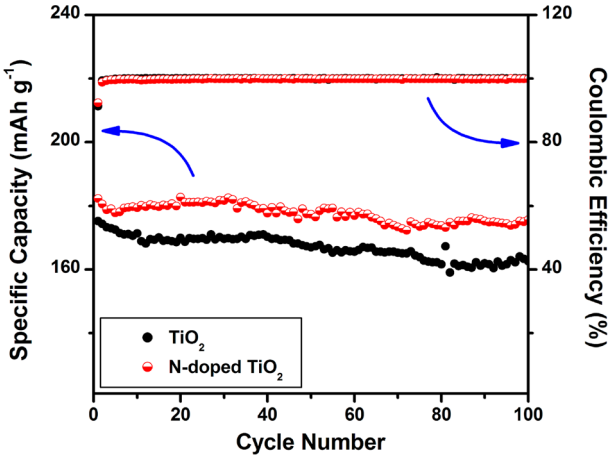

Figure 5. Cycling performance of the TiO_2 and N-doped TiO_2 samples at the 0.2 C rate.

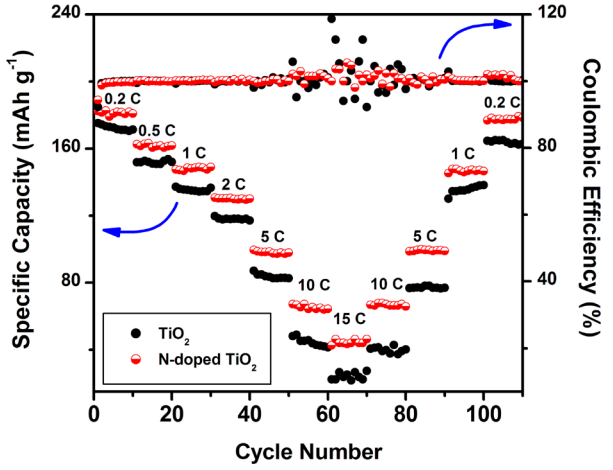

Figure 6. Rate-dependent cycling performance of the TiO_2 and N-doped TiO_2 samples.

rates. For example, a discharge capacity of 45 mAh g^{-1} is obtained at the 15 C rate, which is 80% higher than that of pure TiO_2. In addition, it is noticed that the Columbic efficiency of TiO_2 begins to vibrate above the 10 C rate, while that of N-doped TiO_2 remains stable even at the 15 C rate. This indicates that N-doped TiO_2 has better high rate stability than the undoped material.

3.4. CV. Figure 7 shows the CV curves of TiO_2 and N-doped TiO_2 at different scan rates. All of the CV curves are characterized by a couple of cathodic/anodic peaks, which are due to Li^+ intercalation/deintercalation under the two-phase transition mechanism. The overall shape of the CV curve is maintained well with an increase of the scan rate. The voltage gap between the cathodic and anodic peaks is known as the electrode polarization, which is closely related to the electrical conductivity of the active material.[34,35] The cathodic/anodic voltages for the undoped TiO_2 at a scan rate of 0.4 mV s^{-1} are 2.13/1.62 V, resulting in an electrode polarization of 0.51 V. In a similar manner, the electrode polarization of N-doped TiO_2 is 0.42 V. Obviously, a decrease of the electrode polarization is due to the higher electrical conductivity of N-doped TiO_2.

In addition, the CV measurement can be used to evaluate the diffusion kinetics of intercalation materials via the equation[36]

$$I_p = 2.69 \times 10^5 n^{3/2} S D_{Li}^{1/2} v^{1/2} \Delta C_0 \quad (1)$$

where n is the number of electrons per species reaction, S is the surface area of the electrode, D_{Li} is the chemical diffusion coefficient of Li^+, ΔC_0 is the concentration of Li^+ ions, and v is the scan rate. From the inset of Figure 7, the cathodic current shows a linear relationship versus $(\text{scan rate})^{1/2}$. Therefore, we can approximately compare the chemical diffusion coefficient of TiO_2 and N-doped TiO_2 using the above equation. It shows that the chemical diffusion coefficient of N-doped TiO_2 is about 2 times higher than that of TiO_2. However, the CV measurement, which is based on a dynamic process, is not critical for calculating D_{Li} with high accuracy. In order to obtain more accurate results, GITT or EIS, which can stabilize at nearly thermodynamic equilibrium conditions, must be used.

3.5. GITT. The GITT method, which was first introduced by Weppner and Huggins, has been widely used to determine the chemical diffusion coefficient of Li^+ ions in electrode materials. Using the traditional GITT method, the electrode system is subjected to a small constant current, and potential changes are measured as a function of time. Assuming one-dimensional diffusion in a solid solution electrode without consideration of the ohmic potential drop, double-layer charging, charge-transfer kinetics, and phase transformation, the ion diffusion coefficient can be calculated using Fick's law through the equation[24,37]

dx.doi.org/10.1021/am5002053 | ACS Appl. Mater. Interfaces 2014, 6, 4458−4465

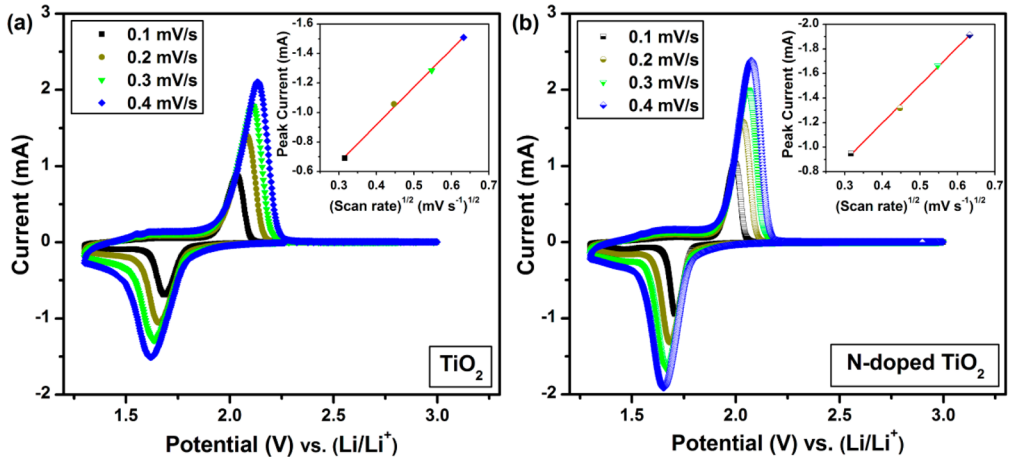

Figure 7. CV curves of the TiO_2 (a) and N-doped TiO_2 (b) samples at different scan rates. Inset: linear fitting of the cathodic current versus (scan rate)$^{1/2}$.

$$D_{Li} = \frac{4}{\pi}\left(I_0\frac{V_m}{FS}\right)^2\left(\frac{dE/dx}{dE/dt^{1/2}}\right)^2 \quad (2)$$

where I_0 is the applied current, V_m is the molar volume of the active material (41.24 cm^3 mol^{-1} for TiO_2), F is the Faraday constant (96485 C mol^{-1}), and S is the surface area of the electrode (0.64 cm^2). Figure 8 shows the GITT curves of TiO_2 and N-doped TiO_2 during the discharge process as a function of the Li^+ content x. The cell was discharged with a current flux of 16.8 mA g^{-1} for an interval of 0.5 h followed by an open-circuit stand for 3 h to allow the cell voltage to reach its quasi-equilibrium value (E_s). The procedure was repeated for the full voltage window of operation. The inset of Figure 8 compares a typical titration step of TiO_2 and N-doped TiO_2 at x = 0.16. It is seen that N-doped TiO_2 has a smaller ohmic polarization and a smaller overpotential, which is due to its higher electrical conductivity. In addition, the N-doped material allows higher Li^+ ion intercalation during each single titration, indicating its better kinetic properties. The evolution of E_s versus x is obtained from the GITT results, as shown in Figure 9. From this figure, the first-order derivative of dE_s/dx as a function of x is obtained as given in the inset of Figure 9. Figure 10 shows an example of E versus $t^{1/2}$ plots recorded for the two materials. It can be seen that, in the time domain from 60 to 300 s, the plot is nearly linear. The slope is taken from this linear range to calculate $dE/dt^{1/2}$. In the inset of Figure 10, we plot the $dE/$

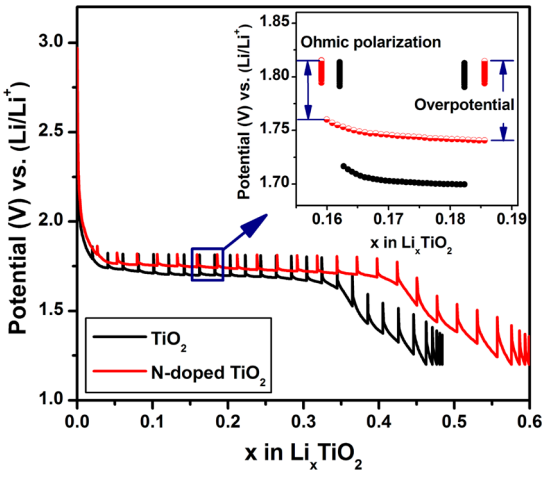

Figure 8. GITT curves of the TiO_2 and N-doped TiO_2 samples as a function of the Li^+ content. Inset: typical titration step of the materials at x = 0.16.

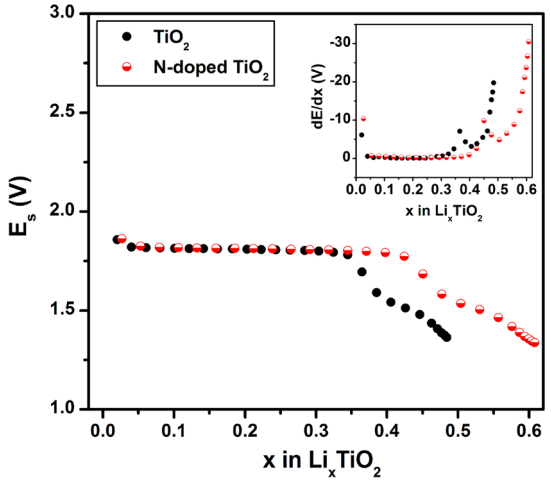

Figure 9. E_s vs x curves of the TiO_2 and N-doped TiO_2 samples. Inset: dE_s/dx values of the samples.

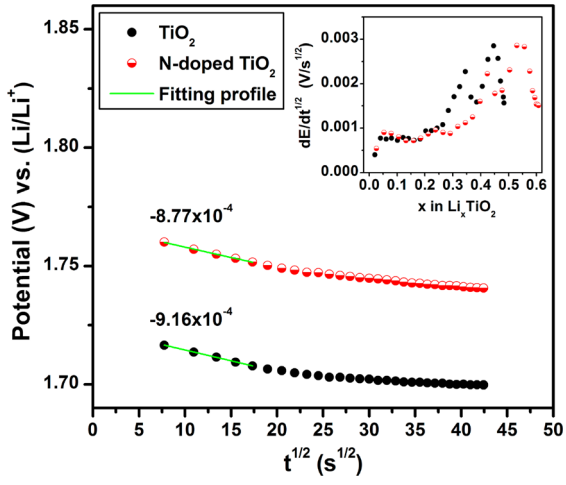

Figure 10. Typical E vs $t^{1/2}$ plot of the TiO_2 and N-doped TiO_2 samples. Inset: $dE/dt^{1/2}$ values of the samples.

dx.doi.org/10.1021/am5002053 | ACS Appl. Mater. Interfaces 2014, 6, 4458−4465

$dt^{1/2}$ values as a function of x of the materials. The chemical diffusion coefficient of Li^+ can be calculated by eq 2 using the values of dE/dx and $dE/dt^{1/2}$. Figure 11 displays the D_{Li} values

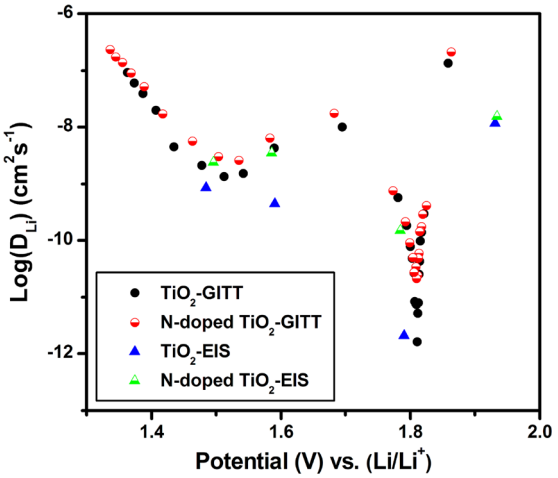

Figure 11. D_{Li} values of the TiO_2 and N-doped TiO_2 samples as a function of the Li^+ content.

of the TiO_2 and N-doped TiO_2 samples as a function of the Li^+ content. It is seen that the variation of D_{Li} strongly depends on the discharge process. Pure TiO_2 has a D_{Li} value of 1.34×10^{-7} cm^2 s^{-1} at the beginning of discharge. Then D_{Li} rapidly decreases and reaches a minimum value of 1.65×10^{-12} cm^2 s^{-1} at the center of the discharge plateau. Afterward, D_{Li} increases to 1.0×10^{-8} cm^2 s^{-1} and then slightly decreases again to 1.34×10^{-9} cm^2 s^{-1}. Finally, D_{Li} increases to 9.06×10^{-8} cm^2 s^{-1} at the end of the discharge. It is seen from Figure 11 that N doping increases the chemical diffusion coefficient of TiO_2. Especially, the minimum D_{Li} at the voltage plateau region is 2.14×10^{-11} cm^2 s^{-1}, about 13 times higher than that of pure TiO_2. This indicates that Li^+ ions can diffuse faster in N-doped TiO_2, which results in its higher capacity and better rate capability.

3.6. EIS. In order to study the electrochemical kinetic properties of the materials, EIS was performed at several typical states of discharge (SODs), i.e., 1.93 V (start of the voltage plateau), 1.79 V (center of the voltage plateau), 1.59 V (end of the voltage plateau), and 1.48 V (lower voltage limit). The Nyquist plots of TiO_2 and N-doped TiO_2 are shown in parts a and b of Figure 12, respectively. From the Nyquist plots, the intercept at the highest frequency is due to the internal resistance (R_s) of the cell arising from the electrolyte, separator, current collector, etc. The semicircle in the high-to-medium-frequency region is majorly due to the charge-transfer process, which can be described by the parallel combination of surface capacitance C_d and charge-transfer resistance R_{ct}. The sloping line in the low-frequency range, called the Warburg region, is due to Li^+ ion diffusion in the electrode bulk. Based on this, the Nyquist plots are simulated using the equivalent circuit, as shown in the insets of Figure 12a,b. First of all, it is seen that the charge-transfer resistance is relatively stable with Li^+ intercalation, only showing a slight decrease at the discharge plateau (1.7 V). R_{ct} of pristine TiO_2 is in the range of 70−81 Ω and then decreases to 41−45 Ω after N doping. The smaller R_{ct} values of N-doped TiO_2 could be due to its larger electrical conductivity.

The Warburg region in the Nyquist plots has been used to determine the chemical diffusion coefficient of Li^+ in electrode materials. By using the model proposed by Ho et al., D_{Li} of TiO_2 can be calculated by the equation[38]

$$D_{Li} = \frac{1}{2}\left[\left(\frac{V_m}{FS\sigma}\right)\left(\frac{dE}{dx}\right)\right]^2 \quad (3)$$

where V_m is the molar volume of TiO_2, S is the surface area of the electrode, F is the Faraday constant, and dE/dx is the first-order derivative of the discharge profile. σ is the Warburg coefficient, which obeys the relationship

$$\sigma = \frac{dZ'}{d\omega^{-1/2}} \quad (4)$$

σ can be obtained from the slope of the linear fitting of Z' versus $\omega^{-1/2}$ plots, as shown in Figure 13. Based on these, the D_{Li} values of TiO_2 and N-doped TiO_2 under different SODs are calculated by eq 3 and are also displayed in Figure 11. It is seen that the D_{Li} values obtained from EIS fit well with those obtained from GITT. This verifies again that N doping improves the Li^+ diffusion coefficient of TiO_2. However, it should be noted that, although the similar results obtained from GITT and EIS establish the validity of both methods, GITT

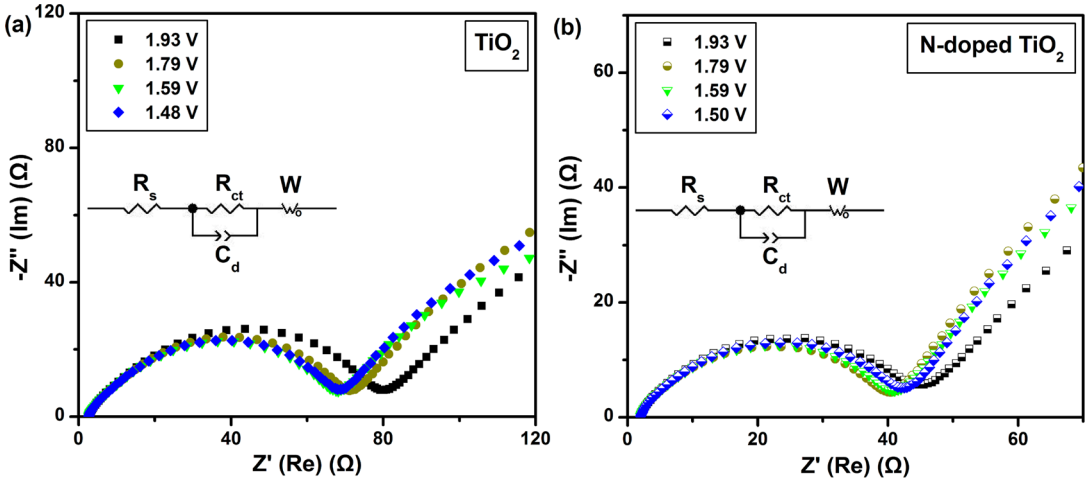

Figure 12. Nyquist plots of the TiO_2 (a) and N-doped TiO_2 (b) samples at different SODs. Inset: equivalent circuit models.

dx.doi.org/10.1021/am5002053 | ACS Appl. Mater. Interfaces 2014, 6, 4458−4465

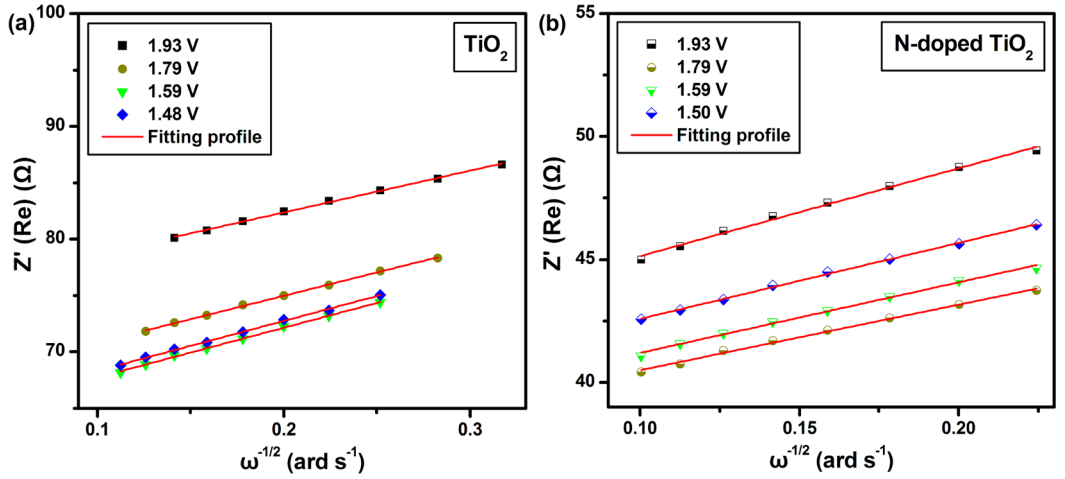

Figure 13. Linear fitting of the Z' vs $\omega^{-1/2}$ relationship of the TiO_2 (a) and N-doped TiO_2 (b) samples at different SODs.

may provide a somewhat more precise result because the ohmic potential drop during GITT titration can be readily eliminated, which guarantees that D_{Li} can be obtained at the most quasi-equilibrium state, as mentioned by Levi and Aurbach.[39,40]

4. CONCLUSIONS

TiO_2 and N-doped TiO_2 nanoparticles have been prepared by a solvethermal method. The N anions reside on the interstitial and substitutional sites in the material bulk, which slightly expands the crystal lattice of TiO_2. The N-doped TiO_2 shows better rate capability than pure TiO_2. A discharge capacity of 45 mAh g^{-1} is obtained at the 15 C rate, which is 80% higher than that of pure TiO_2. The poor rate capability of TiO_2 is attributed to its small lithium diffusion coefficients, which is only 1.65×10^{-12} cm^2 s^{-1} at the center of the discharge plateau. Because most of the discharge capacity is obtained at the discharge plateau, the small lithium diffusion coefficients in this region seriously hinder the specific capacity and rate capability of TiO_2. N doping can improve the lithium diffusion coefficient of TiO_2. Especially, the minimum diffusion coefficient is increased to 2.14×10^{-11} cm^2 s^{-1}, which is 13 times higher than that of pure TiO_2. This substantially improves the specific capacity and rate capability of TiO_2.

AUTHOR INFORMATION

Corresponding Author

*E-mail: yjwei@jlu.edu.cn. Tel and Fax: 86-431-85155126.

Notes

The authors declare no competing financial interest.

ACKNOWLEDGMENTS

This work was supported by the National Natural Science Foundation of China (Grant 51272088), the National Found for Fostering Talents of Basic Science (Grant J1103202), the Research Fund for the Doctoral Program of Higher Education of China (Grant 20110061130006), and the Research Fund for High Technology Development of Jilin Province (Grant 20120310).

REFERENCES

(1) Deng, D.; Kim, M. G.; Lee, J. Y.; Cho, J. Green energy storage materials: Nanostructured TiO_2 and Sn-based anodes for lithium-ion batteries. *Energy Environ. Sci.* **2009**, *2*, 818−837.

(2) Jung, H. G.; Oh, S. W.; Ce, J.; Jayaprakash, N.; Sun, Y. K. Mesoporous TiO_2 nano networks: Anode for high power lithium battery applications. *Electrochem. Commun.* **2009**, *11*, 756−759.

(3) Lee, K. H.; Song, S. W. One-Step Hydrothermal Synthesis of Mesoporous Anatase TiO_2 Microsphere and Interfacial Control for Enhanced Lithium Storage Performance. *ACS Appl. Mater. Interfaces* **2011**, *3*, 3697−3703.

(4) Wang, J.; Zhou, Y.; Hu, Y.; O'Hayre, R.; Shao, Z. Facile Synthesis of Nanocrystalline TiO_2 Mesoporous Microspheres for Lithium-Ion Batteries. *J. Phys. Chem. C* **2011**, *115*, 2529−2536.

(5) Yoon, S.; Manthiram, A. Hollow Core−Shell Mesoporous TiO_2 Spheres for Lithium Ion Storage. *J. Phys. Chem. C* **2011**, *115*, 9410−9416.

(6) Park, S. J.; Kim, H.; Kim, Y. J.; Lee, H. Preparation of carbon-coated TiO_2 nanostructures for lithium-ion batteries. *Electrochim. Acta* **2011**, *56*, 5355−5362.

(7) Lai, C.; Li, G. R.; Dou, Y. Y.; Gao, X. P. Mesoporous polyaniline or polypyrrole/anatase TiO_2 nanocomposite as anode materials for lithium-ion batteries. *Electrochim. Acta* **2010**, *55*, 4567−4572.

(8) Su, X.; Wu, Q.; Zhan, X.; Wu, J.; Wei, S.; Guo, Z. Advanced titania nanostructures and composites for lithium ion battery. *J. Mater. Sci.* **2012**, *47*, 2519−2534.

(9) Guo, Y. G.; Hu, Y. S.; Sigle, W.; Maier, J. Superior electrode performance of nanostructured mesoporous TiO_2 (anatase) through efficient hierarchical mixed conducting networks. *Adv. Mater.* **2007**, *19*, 2087−2091.

(10) Wang, Y.; Li, H.; He, P.; Hosono, E.; Zhou, H. Nano active materials for lithium-ion batteries. *Nanoscale* **2010**, *2*, 1294−1305.

(11) Huang, H.; Zhang, W. K.; Gan, X. P.; Wang, C.; Zhang, L. Electrochemical investigation of TiO_2/carbon nanotubes nanocomposite as anode materials for lithium-ion batteries. *Mater. Lett.* **2007**, *61*, 296−299.

(12) Xin, X.; Zhou, X.; Wu, J.; Yao, X.; Liu, Z. Scalable Synthesis of TiO_2/Graphene Nanostructured Composite with High-Rate Performance for Lithium Ion Batteries. *ACS Nano* **2012**, *6*, 11035−11043.

(13) Fehse, M.; Cavaliere, S.; Lippens, P. E.; Savych, I.; Iadecola, A.; Monconduit, L.; Jones, D. J.; Roziere, J.; Fischer, F.; Tessier, C.; Stievanot, L. Nb-Doped TiO_2 Nanofibers for Lithium Ion Batteries. *J. Phys. Chem. C* **2013**, *117*, 13827−13835.

(14) Ali, Z.; Cha, S. N.; Sohn, J. I.; Shakir, I.; Yan, C.; Kim, J. M.; Kang, D. J. Design and evaluation of novel Zn doped mesoporous TiO_2 based anode material for advanced lithium ion batteries. *J. Mater. Chem.* **2012**, *22*, 17625−17629.

(15) Das, S. K.; Gnanavel, M.; Patel, M. U. M.; Shivakumara, C.; Bhattacharyya, A. J. Anamolously High Lithium Storage in Mesoporous Nanoparticulate Aggregation of Fe^{3+} Doped Anatase Titania. *J. Electrochem. Soc.* **2011**, *158*, A1290−A1297.

(16) Han, H.; Song, T.; Bae, J. Y.; Nazar, L. F.; Kim, H.; Paik, U. Nitridated TiO_2 hollow nanofibers as an anode material for high power lithium ion batteries. *Energy Environ. Sci.* **2011**, *4*, 4532−4536.
(17) Kim, J. G.; Shi, D.; Kong, K. J.; Heo, Y. U.; Kim, J. H.; Jo, M. R.; Lee, Y. C.; Kang, Y. M.; Dou, S. X. Structurally and Electronically Designed TiO_2N_x Nanofibers for Lithium Rechargeable Batteries. *ACS Appl. Mater. Interfaces* **2013**, *5*, 691−696.
(18) Jung, H. G.; Yoon, C. S.; Prakash, J.; Sun, Y. K. Mesoporous Anatase TiO_2 with High Surface Area and Controllable Pore Size by F^--Ion Doping: Applications for High-Power Li-Ion Battery Anode. *J. Phys. Chem. C* **2009**, *113*, 21258−21263.
(19) Wang, Y.; Smarsly, B. M.; Djerdj, I. Niobium Doped TiO_2 with Mesoporosity and Its Application for Lithium Insertion. *Chem. Mater.* **2010**, *22*, 6624−6631.
(20) Jiao, W.; Li, N.; Wang, L.; Wen, L.; Li, F.; Liu, G.; Cheng, H. M. High-rate lithium storage of anatase TiO_2 crystals doped with both nitrogen and sulfur. *Chem. Commun.* **2013**, *49*, 3461−3463.
(21) Asapu, R.; Palla, V. M.; Wang, B.; Guo, Z.; Sadu, R.; Chen, D. H. Phosphorus-doped titania nanotubes with enhanced photocatalytic activity. *J. Photochem. Photobiol. A* **2011**, *225*, 81−87.
(22) Li, Z.; Du, F.; Bie, X.; Zhang, D.; Cai, Y.; Cui, X.; Wang, C.; Chen, G.; Wei, Y. Electrochemical Kinetics of the Li-$[Li_{0.23}Co_{0.3}Mn_{0.47}]O_2$ Cathode Material Studied by GITT and EIS. *J. Phys. Chem. C* **2010**, *114*, 22751−22757.
(23) Delacourt, C.; Ati, M.; Tarascon, J. M. Measurement of Lithium Diffusion Coefficient in $LiyFeSO_4F$. *J. Electrochem. Soc.* **2011**, *158*, A741−A749.
(24) Yang, S.; Wang, X.; Yang, X.; Bai, Y.; Liu, Z.; Shu, H.; Wei, Q. Determination of the chemical diffusion coefficient of lithium ions in spherical $Li[Ni_{0.5}Mn_{0.3}Co_{0.2}]O_2$. *Electrochim. Acta* **2012**, *66*, 88−93.
(25) Xia, H.; Lu, L.; Ceder, G. Li diffusion in $LiCoO_2$ thin films prepared by pulsed laser deposition. *J. Power Sources* **2006**, *159*, 1422−1427.
(26) Yu, Y. P.; Xing, X. J.; Xu, L. M.; Wu, S. X.; Li, S. W. N-derived signals in the x-ray photoelectron spectra of N-doped anatase TiO_2. *J. Appl. Phys.* **2009**, *105*, 123535.
(27) Yin, H. B.; Wada, Y.; Kitamura, T.; Kambe, S.; Murasawa, S.; Mori, H.; Sakata, T.; Yanagida, S. Hydrothermal synthesis of nanosized anatase and rutile TiO_2 using amorphous phase TiO_2. *J. Mater. Chem.* **2001**, *11*, 1694−1703.
(28) Wang, J.; Tafen, D. N.; Lewis, J. P.; Hong, Z.; Manivannan, A.; Zhi, M.; Li, M.; Wu, N. Origin of Photocatalytic Activity of Nitrogen-Doped TiO_2 Nanobelts. *J. Am. Chem. Soc.* **2009**, *131*, 12290−12297.
(29) Valentin, C. D.; Pacchioni, G.; Selloni, A.; Livraghi, S.; Giamello, E. Characterization of paramagnetic species in N-doped TiO_2 powders by EPR spectroscopy and DFT calculations. *J. Phys. Chem. B* **2005**, *109*, 11414−11419.
(30) Saha, N. C.; Tompkins, H. G. Titanium nitride oxidation chemistry: An x-ray photoelectron spectroscopy study. *J. Appl. Phys.* **1992**, *72*, 3072−3079.
(31) Kavan, L.; Kalbáč, M.; Zukalová, M.; Exnar, I.; Lorenzen, V.; Nesper, R.; Graetzel, M. Lithium storage in nanostructured TiO_2 made by hydrothermal growth. *Chem. Mater.* **2004**, *16*, 477−485.
(32) Wagemaker, M.; van Well, A. A.; Kearley, G. J.; Mulder, F. M. The life and times of lithium in anatase TiO_2. *Solid State Ionics* **2004**, *175*, 191−193.
(33) Fröschl, T.; Hörmann, U.; Kubiak, P.; Kučerová, G.; Pfanzelt, M.; Weiss, C. K.; Behm, R. J.; Hüsing, N.; Kaiser, U.; Landfester, K.; Wohlfahrt-Mehrens, M. High surface area crystalline titanium dioxide: potential and limits in electrochemical energy storage and catalysis. *Chem. Soc. Rev.* **2012**, *41*, 5313−5360.
(34) Zhao, H.; Li, Y.; Zhu, Z.; Lin, J.; Tian, Z.; Wang, R. Structural and electrochemical characteristics of $Li_{4-x}Al_xTi_5O_{12}$ as anode material for lithium-ion batteries. *Electrochim. Acta* **2008**, *53*, 7079−7083.
(35) Jiang, T.; Pan, W.; Wang, J.; Bie, X.; Du, F.; Wei, Y.; Wang, C.; Chen, G. Carbon coated $Li_3V_2(PO_4)_3$ cathode material prepared by a PVA assisted sol−gel method. *Electrochim. Acta* **2010**, *55*, 3864−3869.
(36) Das, S. R.; Majumder, S. B.; Katiyar, R. S. Kinetic analysis of the Li^+ ion intercalation behavior of solution derived nano-crystalline lithium manganate thin films. *J. Power Sources* **2005**, *139*, 261−268.
(37) Weppner, W.; Huggins, R. A. Determination of the Kinetic Parameters of Mixed-Conducting Electrodes and Application to the System Li_3Sb. *J. Electrochem. Soc.* **1977**, *124*, 1569−1578.
(38) Ho, C.; Raistrick, I. D.; Huggins, R. A. Application of A−C Techniques to the Study of Lithium Diffusion in Tungsten Trioxide Thin Films. *J. Electrochem. Soc.* **1980**, *127*, 343−350.
(39) Levi, M. D.; Aurbach, D. Frumkin intercalation isotherm—a tool for the description of lithium insertion into host materials: a review. *Electrochim. Acta* **1999**, *45*, 167−185.
(40) Levi, M. D.; Gamolsky, K.; Aurbach, D.; Heider, U.; Oesten, R. Determination of the Li ion chemical diffusion coefficient for the topotactic solid-state reactions occurring via a two-phase or single-phase solid solution pathway. *J. Electroanal. Chem.* **1999**, *477*, 32−40.